

Structure and Infrastructure Engineering

Maintenance, Management, Life-Cycle Design and Performance

ISSN: (Print) (Online) Journal homepage: <https://www.tandfonline.com/loi/nsie20>

Seismic collapse safety assessment of suspended zipper-braced frames

Mohammad Ali Mohammad Taghizadeh & Abbas Karamodin

To cite this article: Mohammad Ali Mohammad Taghizadeh & Abbas Karamodin (28 Oct 2023): Seismic collapse safety assessment of suspended zipper-braced frames, Structure and Infrastructure Engineering, DOI: [10.1080/15732479.2023.2265908](https://doi.org/10.1080/15732479.2023.2265908)

To link to this article: <https://doi.org/10.1080/15732479.2023.2265908>



Published online: 28 Oct 2023.



Submit your article to this journal [↗](#)



View related articles [↗](#)



View Crossmark data [↗](#)



Seismic collapse safety assessment of suspended zipper-braced frames

Mohammad Ali Mohammad Taghizadeh  and Abbas Karamodin 

Department of Civil Engineering, Faculty of Engineering, Ferdowsi University of Mashhad, Mashhad, Iran

ABSTRACT

Seismic evaluation of suspended zipper-braced frames, which are an alternative to inverted-V-braced frames to improve their seismic behavior, is of greatest significance to determine the level of confidence in this type of seismic system during severe earthquakes. The arrangement and design parameters of these frames are mentioned in some references, but there is no probabilistic assessment of collapse risk based on various collapse uncertainties. To evaluate the probability of collapse and margin of safety, eighteen suspended zipper-braced frames with different geometry parameters in the most severe seismic design category (D_{max}) have been designed. The designed frames were modeled in OpenSees software by considering the effect of gusset plate connections and evaluated by performing more than 15,800 dynamic and nonlinear static pushover analyses using FEMA P695 methodology. Total collapse uncertainty is considered in the evaluation of the probabilistic behavior of frames. The results show that the adjusted collapse margin ratio (ACMR) of designed frames by considering the total collapse uncertainty of 0.726 and 0.529 is 27% and 64% higher than the acceptance criteria, respectively. The results also indicate that a response modification coefficient of much more than 6 can be used for the economic design of long-period suspended zipper-braced frames.

ARTICLE HISTORY

Received 24 October 2022
Revised 31 May 2023
Accepted 1 June 2023

KEYWORDS

Collapse uncertainty; incremental dynamic analyses; probabilistic evaluation; safety margin ratio; suspended Zipper-Braced frame

1. Introduction

Concentrically braced frames are one of the foremost effective frames against lateral loads. Among different types which are shown in Figure 1, Chevron Braced Frames play a significant role not only in the face of lateral loads like severe earthquakes but also in mitigating the progressive collapse of other types of structures (Hashemi Rezvani, Mohammad Taghizadeh, & Ronagh, 2019). The performance of such systems is strongly influenced by the behavior of the compression braces.

The buckling of compression braces during severe earthquakes is one of the obvious disadvantages of Chevron Braced Frames, which leads to the localization of failure and sudden drop of lateral resistance of the braced system. Although many methods have been proposed by researchers, such as turning Ordinary Braced Frames into Special Braced Frames by bringing stitches of the bracing members closer together and considering the design requirements of brace connections, the problem of such frames persists in the face of strong earthquakes. The buckling of the compression brace leads to the reduction of its axial capacity, and the axial force in the tension brace increases which results in the emergence of the unbalanced force in the midpoint of the braced beam.

To overcome the problem, Khatib, Mahin, and Pister (1988) suggested a system in which the zipper column located in the middle of the story beams transferred the unbalanced force to other stories, called the Zipper Braced Frame. Since transferring this force results in the buckling

of other compression braces along with the height of the structure, the overall instability is probable (Tirca & Tremblay, 2004). To conquer the undesirable instability, Yang proposed the suspension system through which the top-story braces formed a hat truss. In this system, Suspended Zipper-Braced Frames, the braces located at the top story need to be elastic after buckling of braces in all other stories and form a partial-height zipper mechanism (Yang, 2006).

Many researchers have studied the performance of Zipper Braced Frames (ZBFs) against lateral loads (Kim, Cho, Lee, & Lee, 2008; Schachter & Reinhorn, 2007; Tirca & Tremblay, 2004). Tirca and Chen (2012) investigated the maximum value of axial forces in zippers using several lateral load distribution patterns. Razavi and Sheidaii (2012) substituted a pre-stressed cable for the zipper element. The studied frames were investigated with two pre-stress cables under several scaled ground motions. They concluded that the appropriate pre-stress ratio for cables could improve the performance of Suspended Zipper Braced Frames (SZBFs).

Zahrai, Pirdavari, and Farahani (2013) showed that the Eccentrically Braced Frames (EBFs) system equipped with zipper struts had a stronger tendency to energy dissipation in the plastic zone, 6% higher than that of the regular Eccentrically Braced Frames. Patil and Sangle (2015) compared the behavior of different types of braced frames in a high-rise steel building using nonlinear static analysis, and they showed that the seismic behavior of the Zipper Braced Frame (ZBF) was very close to the V-Braced Frame (VBF)

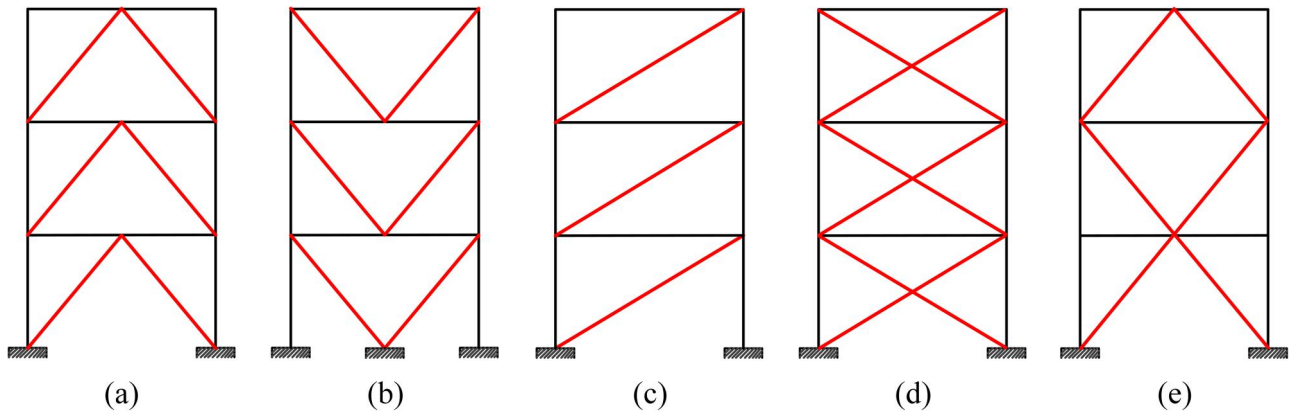


Figure 1. Common types of concentrically braced frames: (a) Chevron Braced Frame (Inverted V-Braced Frame) (b) V-Braced Frame (c) diagonal Braced Frame (d) X-Braced Frame (e) multi story X-Braced Frame.

and Chevron Braced Frame (CBF), in terms of seismic resistance.

Rahimi, Banan, and Banan (2016) compared the seismic behavior of Suspended Zipper Braced Frames (SZBFs) and Zipper Braced Frames (ZBFs) by considering beam-brace connections. The results showed better performance of suspended zipper braced frames than zipper braced frames in tall buildings. Ozcelik, Saritas, and Clayton (2016) investigated the seismic performance of three- and nine-story Suspended Zipper Braced Frames (SZBFs) and Chevron Braced Frame (CBF) using static and dynamic nonlinear analysis. According to the results and in terms of base shear capacities and drift demands, the seismic performance of the three-story SZBF and CBF is very similar, whereas the seismic performance of CBF was better than SZBF in the nine-story building.

The performance of different types of braced frames using static and dynamic nonlinear analyses was compared by Nassani, Hussein, and Mohammed (2017). They showed that Zipper Braced Frame (ZBF), Inverted V-Braced Frame (IVF), and V-Braced Frame (VBF) had not only lower story displacement but also higher seismic performance than other types of studied frames.

Evaluating the seismic behavior of structures against severe earthquakes has always been a far attractive issue among researchers. Asghari and Gandomi (2016) investigated the collapse mechanism of new knee braced frames (KBFs) by comparison with steel moment resisting frames (MRFs). The results indicated that the collapse mechanism of the knee braced frames was similar to the steel moment resisting frames, while the yielding force of MRF was larger than KBF.

Chanda and Debbarma (2021) utilized the incremental dynamic analysis method to assess the seismic response and damage parameters of fixed base and base-isolated reinforced concrete building using near-field and far-field ground motions. They concluded that base-isolated buildings could withstand earthquakes with greater intensity in contrast to fixed base ones. The seismic response assessment of arch bridges was studied by Jahangiri and Yazdani (2021) through the performance-based earthquake engineering

framework using incremental dynamic analyses. The results showed that the span length of arch bridges has the most effect on their seismic behavior.

In recent years, the seismic evaluation and safety margin of various types of structures against a wide range of earthquakes with different frequency content has been investigated by using the framework of FEMA P695 methodology (Applied Technology Council, 2009). Gogus and Wallace (Gogus & Wallace, 2015) assessed the validity of system performance and response parameters of twenty ordinary and twenty special reinforced concrete walls using FEMA P695 Methodology. The results indicated that walls whose height-to-length aspect ratios were 3 or greater could have been designed with a larger response modification coefficient than those suggested in current codes.

Kildashti and Mirghaderi (2017) assessed the response modification coefficient and performance parameters of the complex irregular tower through FEMA P695 methodology and TBI guideline (Pacific Earthquake Engineering Research Center, 2010). Results demonstrated that the R-factor value of 8 was suitable to satisfy the safety against collapse. He, Ou, Li, and Ou (2019) developed a time-variant fiber-reinforced plastics seismic retrofit strategy for corroded reinforced concrete frames using the collapse margin ratio as per FEMA P695.

This paper aims to assess the probabilistic seismic collapse behavior of suspended zipper braced frames with different geometry parameters in the face of a wide variety of earthquakes. To do so, eighteen Suspended Zipper Braced Frames (SZBFs) were designed according to the design requirements of the Seismic Design Category (SDC) D_{max} , and under the framework of FEMA P695 methodology (Applied Technology Council, 2009) over 15,800 dynamic and static analyses were performed to evaluate the margin of safety. To determine the level of confidence, the nonlinear behavior of all structural elements was considered by employing the latest and most efficient nonlinear models of elements such as Post-buckling and the fracture behavior of steel braces in the face of cyclic loading, in-plane rigidity and out-of-plane deformational stiffness of gusset plates.

2. Overall view of seismic collapse assessment method

According to the methodology, the intended building with a lateral load resisting system, called ‘Archetype’, needs to be designed based on predefined response modification coefficient (R) and current codes provisions. Each of these archetypes is assigned to the ‘Performance Group’ that has a common feature in terms of behavioral characteristics, such as the archetype period. In this study, eighteen archetypes were evaluated in six performance groups, considering various brace angles and fundamental periods of archetypes. After designing, nonlinear modeling of archetypes is developed *via* simulation of remarkable deterioration mechanisms that could participate in structural collapse. Because of the impossibility of simulation of all collapse modes in analytical models, the Methodology proposes provisions for evaluating the non-simulated failure modes whose behavior could lead to collapse.

To evaluate the safety margin of investigated archetypes, 44 far-field ground motions are selected for Incremental Dynamic Analyses (Vamvatsikos & Cornell, 2002). The collapse margin of the archetypes, which is the ratio of median collapse intensity to the intensity of the maximum considered earthquake, is obtained from the results of the Incremental Dynamic Analyses (IDA) of each archetype. Finally, the Adjusted Collapse Margin Ratio (ACMR), modifications due to spectral shape effects, is compared with the acceptance criteria introduced in the methodology based on various sources of uncertainty. If the Adjusted Collapse Margin Ratio meets the acceptance criteria, the safety margin of designed archetypes is considered acceptable.

3. Design requirements of archetypes

Force-resisting systems of all archetypes need to be designed to have adequate strength and stiffness in the face of intended earthquake ground motion. Accordingly, seismic forces were determined *via* two methods of equivalent

lateral force and response spectrum analysis. Each archetype was designed with either of these two methods and finally, the most economical design was selected. To evaluate the seismic performance of Suspended Zipper Braced Frames (SZBFs), eighteen archetypes were designed. As shown in Figure 2, the plan of archetypes consisted of six spans of 6, 7, and 8 meters, two of which are equipped with perimeter braced frames. Archetypes were 2, 3, 6, 9, 12, and 15-stories with a story height of 3.6 meters as indicated in Figure 3.

Minimizing the damage to the building components and ensuring the functionality of the building during severe earthquakes, the ASCE/SEI 7-10 limits the drift ratio to 2%. So to satisfy the limit, four braced bays were located in each perimeter frame of the 15-story archetype (ASCE/SEI 7-10, 2013). In this study, the identification code of archetypes is based on the number of stories and the span length. For example, the archetype 15Z8S refers to the 15-story archetype with a span length of 8 meters.

The distributed dead load of 5.0 kN/m^2 was considered for floors, while its value was 4.5 kN/m^2 for the roof. The floor and roof live load was 2.4 and 0.96 kN/m^2 , respectively. The wall load for perimeter frames was assumed to be 6.5 kN/m . ASTM A992 material with the yield and ultimate tensile strength of 345 MPa and 448 MPa, respectively, was considered for W-shape sections. The ASTM A572 was assumed for gusset plate material ($F_y = 345 \text{ MPa}$, $F_u = 448 \text{ MPa}$). The values of R_y for the ASTM A992 and ASTM A572 was 1.1 as per AISC 341-10 (AISC 341-10, 2010). ASTM A500 Gr. B material with the R_y value of 1.4 whose yield and ultimate tensile strength were 315 MPa and 400 MPa, respectively, was expected for square hollow structural sections (HSS).

For 2-, 3- and 6-story archetypes, the lateral seismic forces were calculated from the Equivalent Lateral Force (ELF) method. Because of the optimal design in taller archetypes and the limitation of using the Equivalent Lateral Force procedure in seismic design category D_{\max} , the Response Spectrum Analysis (RSA) procedure was selected for 9-, 12- and 15-story. According to the Equivalent Lateral Force (ELF) method, seismic base shear was calculated

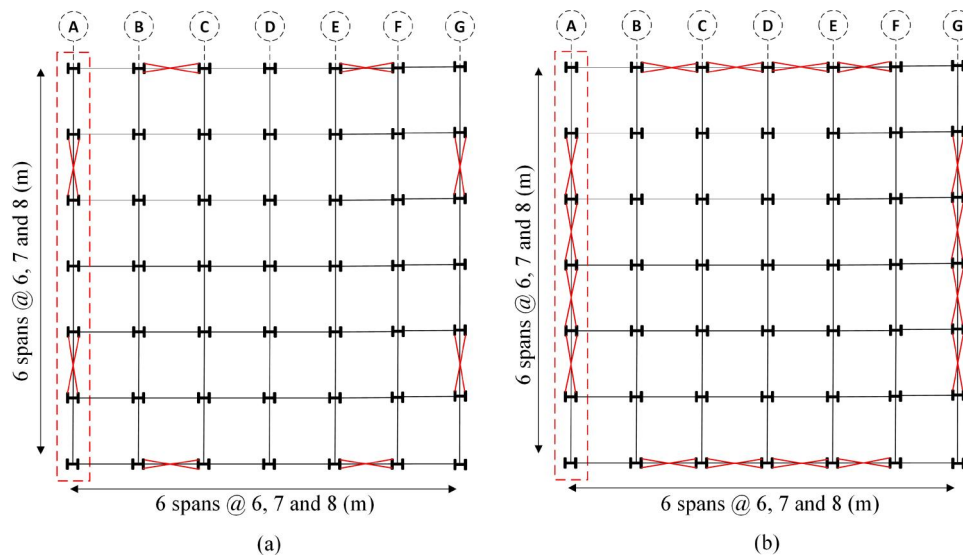


Figure 2. Plan view of SZBFs: (a) 2-, 3-, 6-, 9- and 12-story archetypes (b) 15-story archetype.

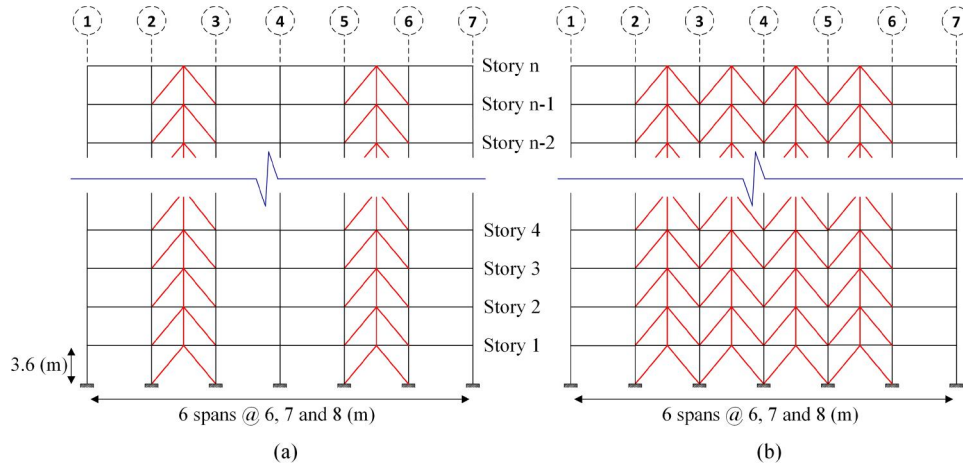


Figure 3. Elevation view of SZBFs: (a) 2-, 3-, 6-, 9- and 12-story archetypes (b) 15- story archetype.

Table 1. Seismic design parameters.

Archetype	Gravity loads	Seismic design methods	S1 (g), SD1 (g),	Ss (g), SMS(g)	T(s)	V/W	SMT(g)
2-story	Typical	ELF	0.6	1.5	0.3	0.1667	1.5
3-story	Typical	ELF	0.6	1.5	0.4070	0.1667	1.5
6-story	Typical	ELF	0.6	1.5	0.6845	0.1462	1.31
9-story	Typical	RSA	0.6	1.5	0.9278	0.0864	0.97
12-story	Typical	RSA	0.6	1.5	1.1512	0.0703	0.78
15-story	Typical	RSA	0.6	1.5	1.3609	0.0557	0.66

based on the seismic response coefficient factor. All limitation related to the maximum and minimum value of this factor was observed following the requirements of Section 12.8.1.1 of ASCE/SEI 7-10.

The fundamental period of archetypes ($T = C_u \times T_a$) was used in defining seismic forces and collapse spectral intensity. Design parameters based on the Seismic Design Category (SDC) which is specified as the level of the design earthquake ground motion and the risk category of the archetype are provided in Table 1. To do so, the SDC D_{max} was considered with the $S_{DS} = 1.0g$ and $S_{D1} = 0.60g$ (ASCE/SEI 7-10, 2013).

In the RSA procedure, seismic forces were obtained from a modal response spectrum analysis which is a linear dynamic analysis using the calculated fundamental period of archetypes. Natural modes of archetypes were determined by performing dynamic analyses, considering modal mass participation of more than 90% in each direction. SRSS method was selected to combine different modes. the combined response for the modal base shear (V_{RSA}) should not be considered less than base shear forces using the equivalent lateral force method ($V = C_s \times W$). If the modal base shear derived from combined responses was less than base shear forces (V), all designed forces and drift ratios were multiplied by the ratio of $\beta = 0.85 \times (V/V_{RSA})$ as per ASCE/SEI 7-10.

No Irregularities are considered in the plan or height of archetypes. According to the methodology, two assumptions were taken into the account: (1) The redundancy factor (ρ) was equal to 1.0 for conservative collapse assessment, and (2) the deflection amplification factor (C_d) which actually

represents the ratio of the maximum inelastic displacement to the elastic one during an earthquake was assumed to be equal to the response modification coefficient in the process of controlling drift ratios.

All archetypes were designed in two phases of strength and capacity (Yang, Leon, & DesRoches, 2008). In the strength design phase and before adding zipper elements, all the braces except top story braces were designed as per Special Concentrically Braced Frames (SCBF) (AISC 341-10, 2010). Accordingly, width-to-thickness ratios of brace sections were assumed to be lower than λ_{hd} .

Braces were connected to columns and beams through gusset plates designed by the uniform force method as discussed in the AISC Steel Construction Manual (Muir & Duncan, 2011). So as to perform plastic hinges and out-of-plane buckling, a free length of $2t$ was assumed between the fold line of the gusset plate and the end of the brace element, where t was taken as the thickness of the gusset plate. The compression brace strength was expected to be equal to lesser of $R_y F_y A_g$ and $1.14 F_{cre} A_g$ (AISC 341-10, 2010). Beams were designed in the absence of shear forces resulting from the unbalanced forces in this phase.

In the capacity phase, other structural elements, including roof braces, columns, zipper elements, beams, and bracing connections were designed (Yang, Leon, & DesRoches, 2008). Braces between the two upper floors were designed with the assumption of elastic behavior to prevent the occurrence of dynamic instability of the structure in the face of severe earthquakes. Beams must be designed to withstand the horizontal component of axial forces created in adjacent

braces and flexural moments induced by gravitational and seismic forces.

In order to transfer the unbalanced force induced by buckling of the compression braces to upper stories, zipper struts were located at the intersection of tension and compression braces between all adjacent stories. Accordingly, the zipper struts needed to resist all unbalanced forces created by the braces inserted on the level below. Finally, all columns must be designed in such a way that they were able to transfer all the forces transmitted by the braces and zipper elements to the foundation. All designed elements of archetypes are provided in [Appendix A](#).

4. Nonlinear modeling of archetypes

The nonlinear behavior of all structural elements was considered by implementing the OpenSees framework (Mazzoni, McKenna, Scott, & Fenves, 2006). The material behavior for all members was simulated by Steel02 material which is an available material model in OpenSees library, Giuffre-Menegotto-Pinto model. The yield stress, Young's modulus, strain-hardening ratio, and empirical parameters which determine the transition of the elastic to the plastic behavior are the most important parameters which define the monotonic curve of this material. To do so, The proposed parameters of the recent investigation (Karamanci & Lignos, 2014) were used to calibrate the analytical modeling of the material. The suggested parameters, R_0 , cR_1 , and cR_2 whose values form the nonlinear behavior of steel material from the elastic to plastic branch as well as cyclic hardening parameters, a_1 , a_2 , a_3 , and a_4 are provided in [Table 2](#).

The nonlinear behavior of columns and beams was considered by employing a fiber beam-column model based on the iterative force-based formulation. Depending on the cross section shape, various discretization was utilized. Hence, for w-shape sections, two fibers through the thickness of the flange and web, six fibers along the flange width, and web depth were used. Similarly, for square HSS sections, four fibers through the cross-sectional thickness and ten fibers along the flange were considered.

A co-rotational formulation was embedded in the analytical model to consider large displacements. To simulate the second-order effects, a leaning column, as the gravity framing system, with no lateral strength and stiffness was considered. The portion of gravity load distributed on each floor was applied to the leaning column as the axial gravity load. As shown in [Figure 4](#), rigid links and rotational springs

were intended as the connection between the leaning column and the archetype frame.

The most significant part of nonlinear modeling is the simulation of the hysteretic response of steel braces in the face of cyclic loading. In this study, Numerical modeling of Post-buckling and the fracture behavior of steel braces were modeled according to the proposed method of Uriz, Filippou, and Mahin (2008). Large plastic strains before the failure of steel braces caused by stresses greater than the yield strength of the material were simulated by fatigue material, low cycle fatigue which is available in the library of OpenSees software. Accordingly, the fracture of steel concentrically braces under the definite number of cycles was considered by a modified rainflow cycle counter algorithm with a linear strain accumulation of damage using Miner's Rule.

Steel material can withstand a large number of cycles before experiencing fatigue failure. However, fatigue material models implemented in the modeling process specifically account for low-cycle fatigue, which occurs at relatively small numbers of cycles but high stress amplitudes, to track damage accumulation and strain amplitudes in each fiber of the section.

For slender cross sections, local buckling can substantially increase local strain demands, leading to a further reduction in the fatigue life of brace elements. Experimental studies indicate that the hysteretic response of the brace under cyclic loading is not significantly affected by local buckling, provided that the section is compact (Uriz, 2005). Moreover, some research studies have shown that a lower width-to-thickness ratio contributes to greater ductility, resulting in the delayed occurrence of localized buckling in bracing members under cyclic loading (Fell, Kanvinde, Deierlein, Myers, & Fu, 2006).

Table 2. Recommended parameters for analytical modeling of the steel material (Karamanci & Lignos, 2014).

Modeling parameters		Square HSS section	W-shape section
strain-hardening ratio	b	0.001	0.00100
Steel material (Giuffre-Menegotto-Pinto)	R0	22.0	20.0
	cR1	0.925	0.925
	cR2	0.250	0.250
	a1	0.030	0.010
	a2	1.000	1.000
	a3	0.020	0.020
	a4	1.000	1.000

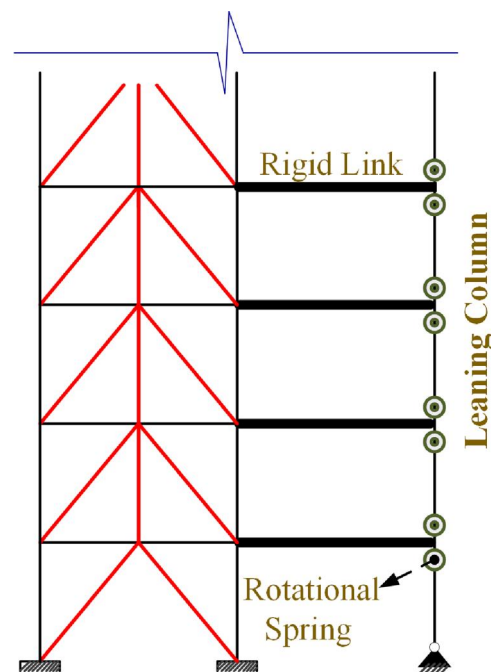


Figure 4. Schematic modeling of leaning column.

In order to prolong the fatigue life of steel braces and ensure their capacity retention under intense cyclic loading, seismic provisions for structural steel buildings (AISC 341-10, 2010) impose restrictions on the width-to-thickness ratios of brace sections in concentrically braced frames located in regions with high seismic risk. Accordingly, the width-to-thickness limitation (λ) outlined in AISC 341-10 was implemented, ensuring that all selected members were categorized as highly ductile members ($\lambda \leq \lambda_{hd}$).

Global buckling of the steel braces was simulated by considering an initial imperfection of $0.001L$ in the midpoint of steel braces which corresponded to the experimental data calibration (Karamanci & Lignos, 2014). The bracing connections to other structural elements, gusset plates, were modeled by placing the rotational nonlinear springs at the end of braces. As shown in Figure 5, the in-plane rigidity and out-of-plane deformational stiffness of gusset plates were considered in the numerical model by rigid links and zero-length nonlinear rotational springs, respectively. The initial stiffness of the rotational springs was defined according to the investigation of Hsiao et al. based on Whitmore's width, buckling lengths, thickness, and the material properties of gusset plates (Hsiao, Lehman, & Roeder, 2012).

Assessing of collapse margin ratio is highly dependent on the accuracy of the analytical model. Hence, nonlinear modeling of archetypes must be accurate enough to predict structural failure in the face of a variety of loads. Accordingly, effective failure modes of steel braces as previously described were implemented in the nonlinear modeling of archetypes by considering gusset plate connection.

The capability of the model in capturing the post-buckling behavior of steel braces under earthquake ground motions was investigated by comparing the nonlinear model with experimental data. To do so, the result of the dynamic analysis of the nonlinear model of one story chevron concentrically braced frame simulated in the OpenSees platform was compared with the experimental data obtained from the results of the shake table test performed in the E-Defense laboratory (Okazaki, Lignos, Hikino, & Kajiwara, 2013). Figure 6 indicates the good accuracy of the analytical model to trace the cyclic response and fracture of the steel brace.

5. Seismic collapse evaluation

To assess the collapse margin ratio of Suspended Zipper Braced Frames (SZBFs), eighteen archetypes were designed according to the design requirements as described in the previous sections. After designing, nonlinear models were developed based on calibrated model. Baker and Cornell indicated that some rare ground motions had different spectral shapes in comparison with the intended design spectrum in ASCE/SEI 7-10 as a result of their inherent peaked shape at the target of interest (Baker & Allin Cornell, 2006).

Spectral shape factors whose values depend on the period-based ductility and fundamental period were defined in the methodology to account for spectral shape effects. Table 7-1b of FEMA P695 provides the values of spectral shape factors according to the period-based ductility and the fundamental period of archetypes (Applied Technology Council, 2009). To do so, nonlinear static pushover analysis with a lateral load distribution based on the fundamental mode shape of archetypes was performed to estimate the ratio of the ultimate roof displacement to the effective yield roof displacement defined as the period-based ductility ($\mu_t = \delta_u / \delta_{y,eff}$).

The collapse capacity of archetypes was assessed by performing nonlinear dynamic analyses with a wide range of earthquake ground motions, a set of 44 far-field ground motions as described in the methodology. The necessary element of nonlinear dynamic analysis was the scaling of ground motion records. The scaling process included two stages: I. normalization and II. scaling. As per FEMA P695 (Applied Technology Council, 2009), individual records of the far-field record set were normalized by their respective peak ground velocities. Finally, normalized ground motions were scaled to increasing earthquake intensities until half of the records in the far-field record set caused the collapse of an archetype model. To do so, incremental dynamic analysis (IDA) was performed.

Among many quantities that had been proposed to characterize the 'intensity' of a ground motion record, the 5% damped spectral acceleration at the archetype's fundamental period, $S_T(T)[g]$, was selected as the intensity measure, IM. In this study, instead of using a constant step for increasing the intensity measure, the Hunt-fill algorithm was used to

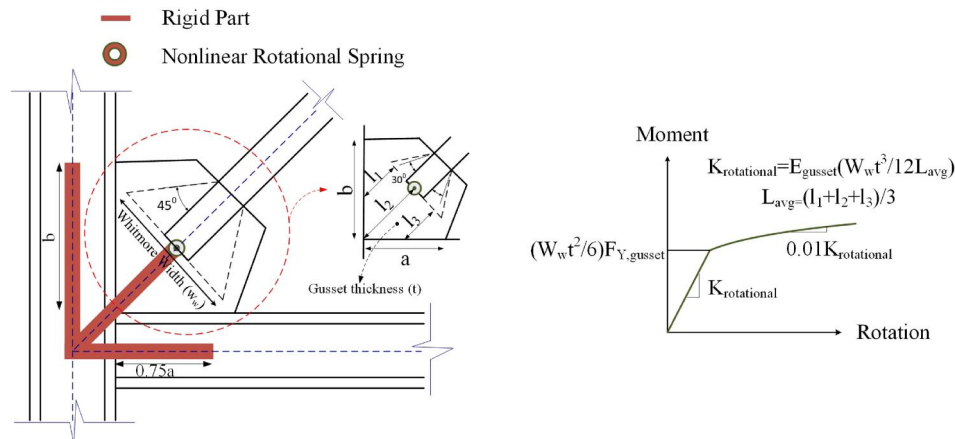


Figure 5. Representation of gusset plate connection model (Hsiao et al., 2012).

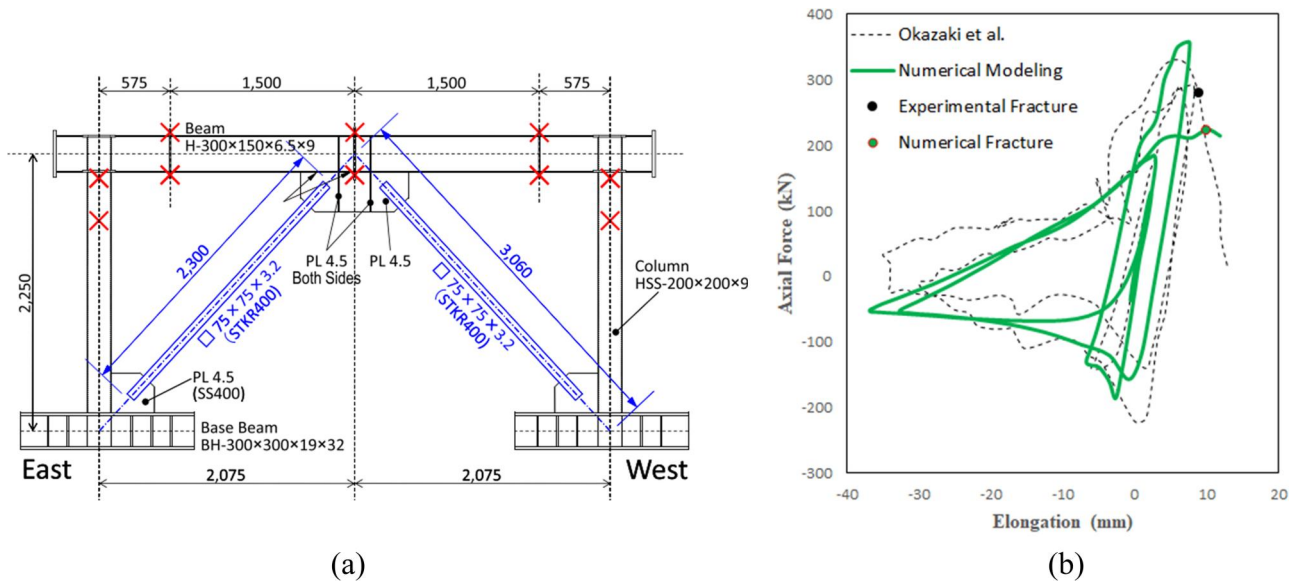


Figure 6. Bracing element verification: (a) configuration of the frame (all dimensions in mm) (Okazaki et al., 2013) (b) comparison of numerical modeling and experimental test data.

locate the capacity point of the archetype optimally (Vamvatsikos & Cornell, 2002). As explained before, important failure modes such as global buckling and the fracture of braces were simulated in the analytical model explicitly. Due to the inherent limitations in considering all failure modes in the numerical models, the non-simulated failure criteria of 10% story drift capacity of Suspended Zipper Braced Frames (SZBFs) was also selected to incorporate column failure mode in the evaluation. The ratio of the spectral acceleration in which 50% of archetypes collapsed (\hat{S}_{CT}) to the spectral acceleration of the maximum considered earthquake ground motions (S_{MT}) determines the Collapse Margin Ratio ($CMR = \hat{S}_{CT}/S_{MT}$) of the frames.

To better understand the process of the collapse evaluation, the Incremental Dynamic Analyses (IDA) results of performance groups PG-1 (the archetypes 2Z6S and 3Z6S) and PG-2 (the archetypes 6Z6S, 9Z6S, 12Z6S, and 15Z6S) are shown in Figure 7. The \hat{S}_{CT} varies from 4.63 g to 2.41 g. Taking into account some exceptions in the results obtained from the IDA results of archetype with the span length of 6, 7, and 8 meters, there was a slight tendency between archetype heights and \hat{S}_{CT} so that with the increase in the height of the archetypes, the median collapse capacity of the archetypes decreased. It is worth mentioning that the relative value of this coefficient to the S_{MT} is a decisive factor. Among all archetypes with a span of 6 meters, the highest Collapse Margin Ratio (CMR) is for the archetype 12Z6S with a value of 4.12, while the lowest is for the archetype 2Z6S with a value of 2.07.

The collapse fragility data of all studied archetypes is indicated in Figure 8. fragility curves indicate the collapse probability as a function of an intensity measure, spectral response acceleration at the fundamental period. A lognormal distribution is fitted through the collapse data as well. The median collapse intensity corresponded to the 50% probability of the collapse was calculated for each

performance group. The archetype 3Z6S has the highest value of \hat{S}_{CT} among all performance groups ($\hat{S}_{CT} = 4.63g$), whereas the archetype 12Z6S has the highest value of CMR equal to 4.12. The reason the higher value of \hat{S}_{CT} does not provide a greater margin of safety is that the CMR of archetypes depends not only on median collapse intensity but also on the maximum considered earthquake as the ground motion demand. The lowest Collapse Margin Ratio (CMR) in all studied archetypes belongs to the 2-story archetype, while the 12-story archetype has the highest value.

The collapse margin ratio was adjusted for each archetype by spectral shape factor (SSF) which is a function of the period-based ductility (μ_T), fundamental period (T), and seismic design category, as described before ($ACMR_i = CMR_i \times SSF$). Adjusted Collapse Margin Ratios ($ACMRs$) need to be evaluated by the predefined values introduced as acceptance criteria in the methodology. Many factors affect collapse margin ratios such as uncertainties in construction, design, and analysis of archetypes. Hence, the collapse assessment process must be followed by considering four main sources of uncertainties whose quality ratings affect collapse assessment, including design requirements uncertainty (β_{DR}), test data uncertainty (β_{TD}), modeling uncertainty (β_{MDL}), and Record-to-Record uncertainty (β_{RTR}).

In this study, the quality rating of design requirements, experimental data, and the accuracy of the nonlinear model was determined as 'good' with the quantitative value of 0.2 following the methodology (Applied Technology Council, 2009). The proposed value of β_{RTR} defined as Record-to-Record uncertainty is 0.4 as explained elsewhere (Applied Technology Council, 2009). Because of the independency of four sources of uncertainties, the total system collapse uncertainty is defined as the square root of the sum of squares of each uncertainty ($\beta_{TOT} = \sqrt{\beta_{DR}^2 + \beta_{TD}^2 + \beta_{MDL}^2 + \beta_{RTR}^2}$). Considering the foregoing, the total system collapse uncertainty is 0.52, but for considering greater uncertainty in the

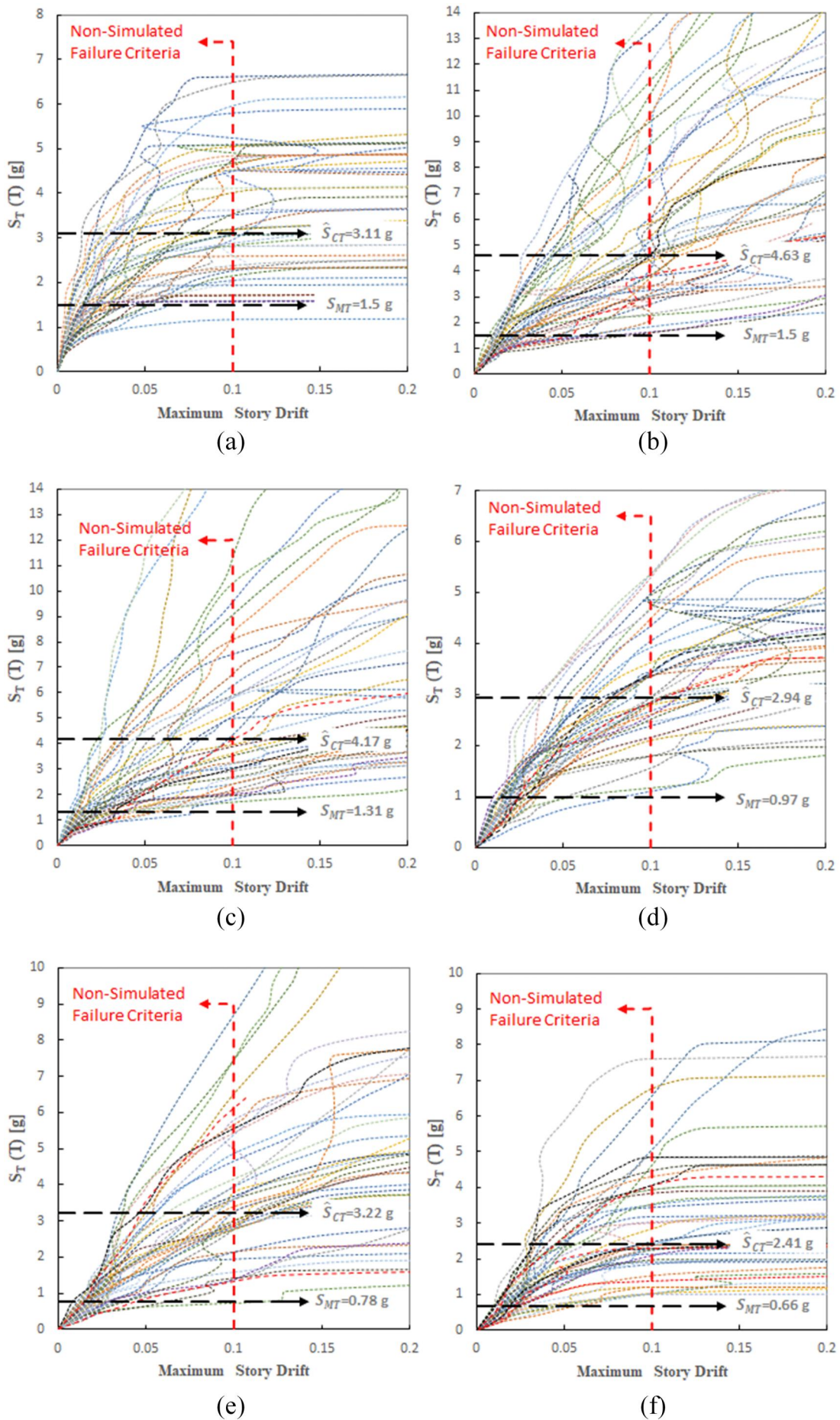


Figure 7. IDA curves: (a) 2Z6S; (b) 3Z6S; (c) 6Z6S; (d) 9Z6S; (e) 12Z6S; (f) 15Z6S.

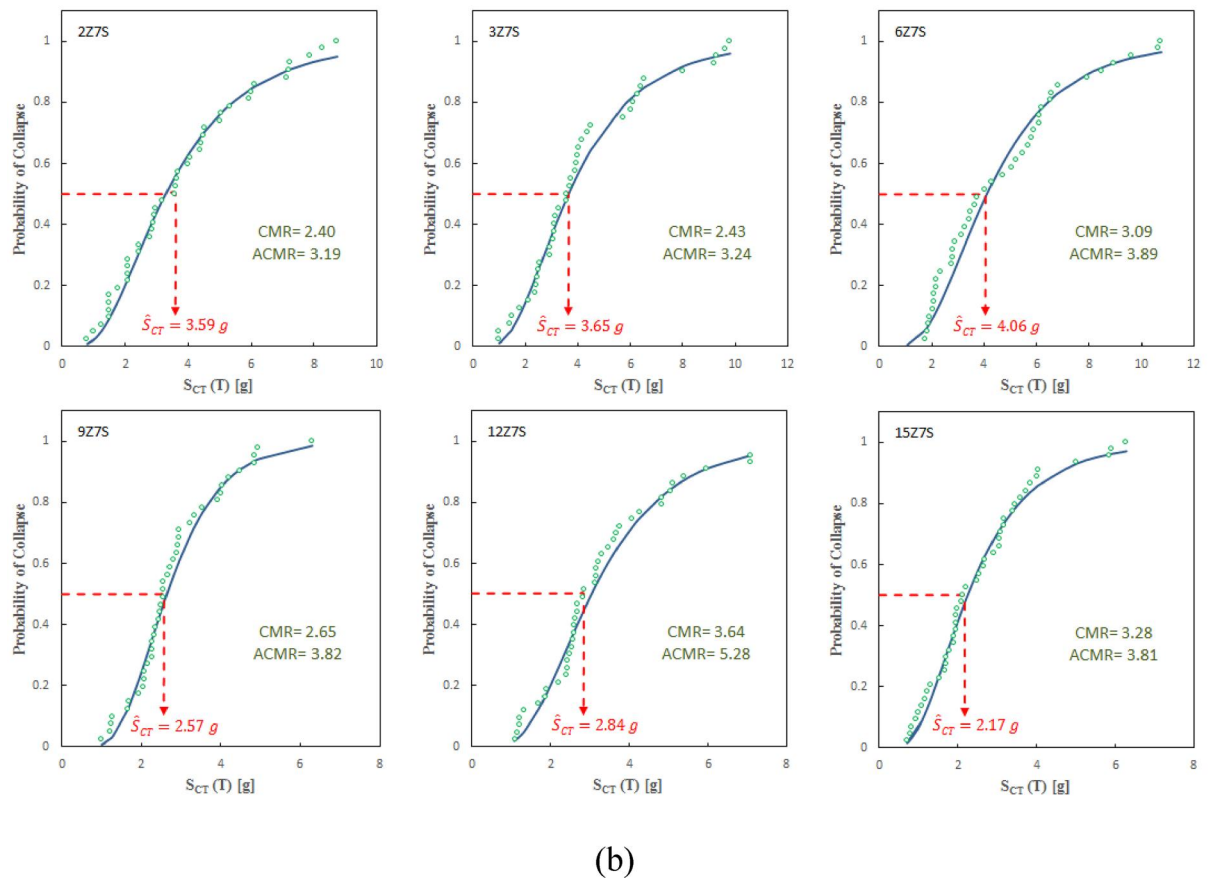
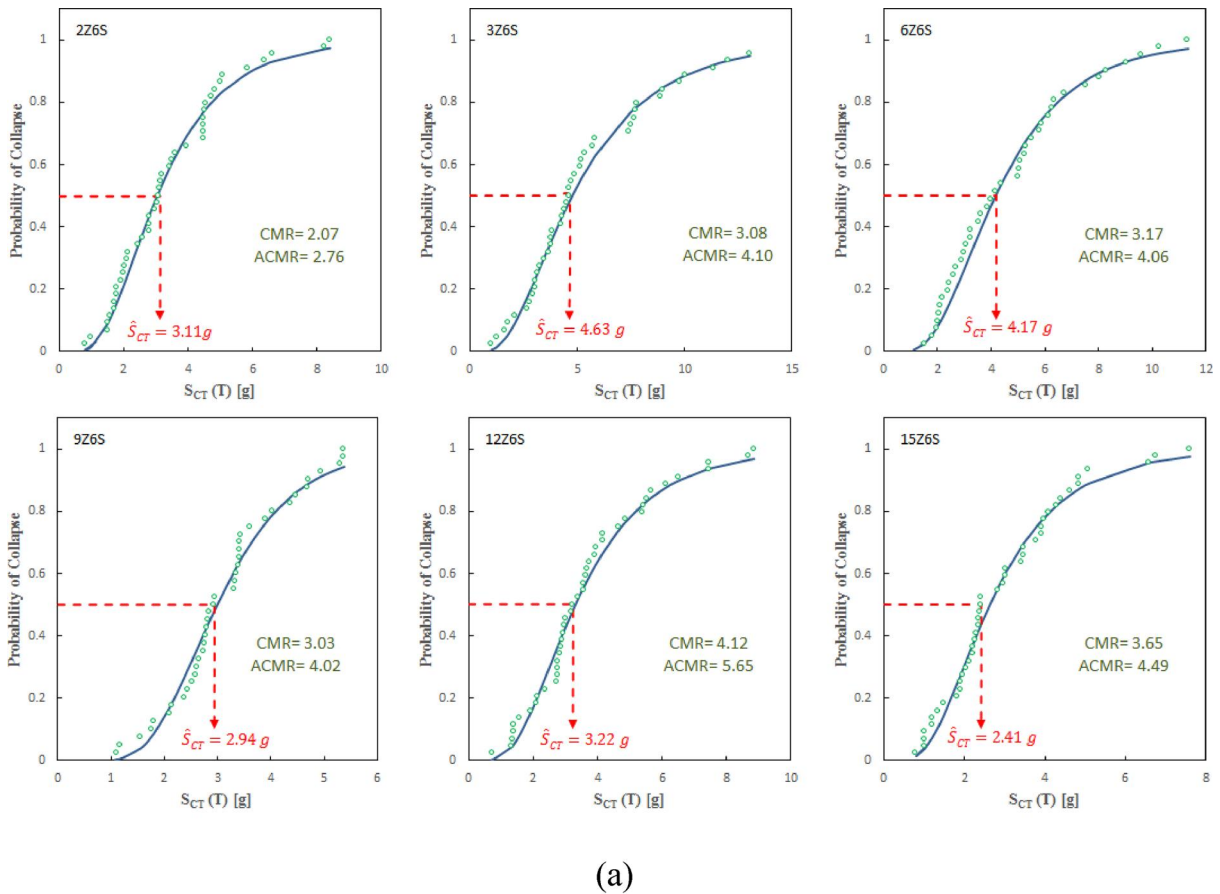
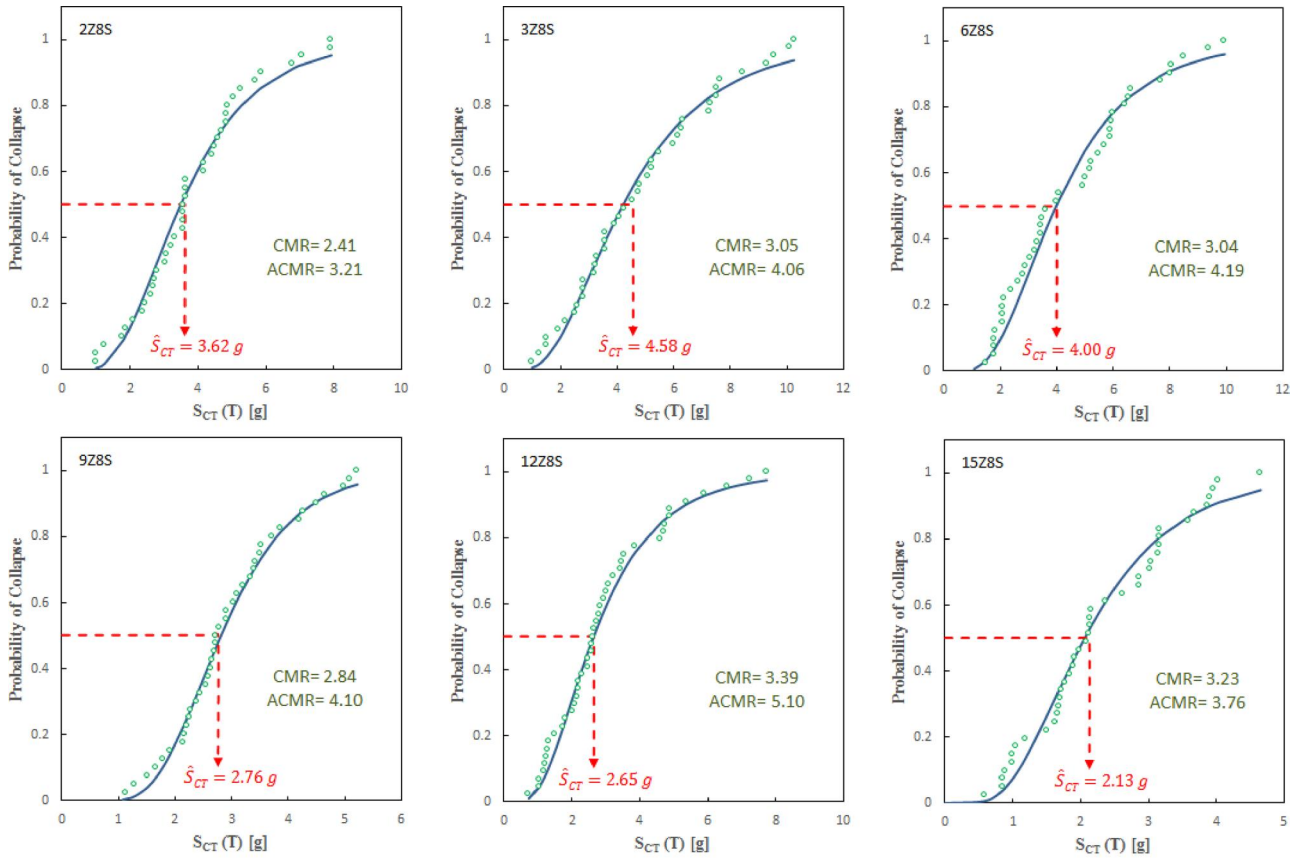


Figure 8. Fragility curves of performance groups: (a) PG-1 and PG-2; (b) PG-3 and PG-4; (c) PG-5 and PG-6.



(c)

Figure 8. Continued.

collapse assessment process, the total collapse uncertainty of 0.726 has also been considered due to the ‘fair’ rating of design requirements, experimental data, and the accuracy of the nonlinear model ($\beta_{DR} = \beta_{TD} = \beta_{MDL} = 0.35$).

To pass the acceptance criteria, the calculated Adjusted Collapse Margin Ratios (ACMRs) and their average values for each performance group need to be greater than the acceptance criteria of $ACMR_{20\%}$ and $ACMR_{10\%}$, respectively. Otherwise, the seismic performance of intended archetypes is not acceptable. Table 7-3 of FEMA P695 gives the predefined values of $ACMR_{20\%}$ and $ACMR_{10\%}$ based on the total system collapse uncertainty (Applied Technology Council, 2009). Moreover, these predefined values and the summary collapse performance of Suspended Zipper Braced Frames are provided in Table 3.

It is observed from Table 3 that the average Adjusted Collapse Margin Ratios (ACMRs) in performance groups (ACMRs) of the long-period archetypes are higher than in performance groups of the short-period archetypes. Moreover, the ACMRs indicate that the considered range of span lengths (6, 7, and 8 meters) and brace angles (50.19, 45.81, and 41.99 degrees) in the Suspended Zipper Braced Frames did not have much effect on the average adjusted collapse margin ratio. The results show that all designed archetypes with the predetermined response modification factor of 6 have passed the acceptance criteria of the methodology.

The lowest safety margin of performance groups belongs to the PG-3 which is 64% and 27% higher than the acceptance criteria defined for $\beta_{TOT} = 0.529$ and $\beta_{TOT} = 0.726$, respectively. On the other hand, the average Adjusted Collapse Margin Ratio (ACMR) of PG-2, long-period archetypes with a span of 6 meters, is more than the acceptance criteria with a significant difference. The index archetype of each performance group has passed the acceptance process of the methodology, as well.

While the archetype 2Z6S (as defined in Table 3) has the lowest ACMR, its adjusted safety margin ratio is 77% and 50% higher than the acceptance criteria corresponding to the total uncertainties of 0.526 and 0.726. As per methodology, the value of overstrength factor was considered as the largest average value of calculated overstrength of any performance group. Hence, Suspended Zipper Braced Frame (SZBF) overstrength factor (Ω_0) is taken 2.5, after rounding to the nearest half unit as specified in FEMA P695.

6. Conclusion

The collapse performance of Suspended Zipper Braced Frames (SZBFs) was studied using FEMA P695 methodology. Eighteen archetypes were designed with the predetermined response modification factor of 6, similar to the factor for the Special Steel Concentrically Braced Frame

Table 3. Collapse assessment of archetypes.

Archetype identification	Design configuration			Nonlinear analyses results					Acceptance criteria		
	Number of story	Total Height (m)	Static Ω	$S_{MR}(g)$	$\hat{S}_{CT}(g)$	μ_T	SSF	ACMR	Acceptable ACMR $\beta_{TOT} = 0.529$	Acceptable ACMR $\beta_{TOT} = 0.726$	Fail/Pass
2Z6S	2	7.2	2.24	1.5	3.11	16.97	1.33	2.76	ACMR _{20%} 1.56	ACMR _{20%} 1.84	Pass
3Z6S	3	10.8	2.06	1.5	4.63	11.31	1.33	4.10	ACMR _{10%} 1.96	ACMR _{10%} 2.53	Pass
Mean of performance group			2.15					3.43			Pass
6Z6S	6	21.6	2.55	1.31	4.17	4.95	1.28	4.06	ACMR _{20%} 1.56	ACMR _{20%} 1.84	Pass
9Z6S	9	32.4	2.06	0.97	2.94	4.70	1.32	4.0	ACMR _{20%} 1.56	ACMR _{20%} 1.84	Pass
12Z6S	12	43.2	2.28	0.78	3.22	4.93	1.37	5.65	ACMR _{10%} 1.96	ACMR _{10%} 2.53	Pass
15Z6S	15	54	2.74	0.66	2.41	2.22	1.23	4.49	ACMR _{10%} 1.96	ACMR _{10%} 2.53	Pass
Mean of performance group			2.41					4.55			Pass
2Z7S	2	7.2	1.95	1.5	3.59	17.75	1.33	3.19	ACMR _{20%} 1.56	ACMR _{20%} 1.84	Pass
3Z7S	3	10.8	2.07	1.5	3.65	15.65	1.33	3.24	ACMR _{10%} 1.96	ACMR _{10%} 2.53	Pass
Mean of performance group			2.01					3.21			Pass
6Z7S	6	21.6	2.16	1.31	4.06	4.32	1.26	3.89	ACMR _{20%} 1.56	ACMR _{20%} 1.84	Pass
9Z7S	9	32.4	1.70	0.97	2.57	10.59	1.44	3.82	ACMR _{20%} 1.56	ACMR _{20%} 1.84	Pass
12Z7S	12	43.2	1.81	0.78	2.84	6.64	1.45	5.28	ACMR _{10%} 1.96	ACMR _{10%} 2.53	Pass
15Z7S	15	54	2.00	0.66	2.17	1.52	1.16	3.81	ACMR _{10%} 1.96	ACMR _{10%} 2.53	Pass
Mean of performance group			1.92					4.2			Pass
2Z8S	2	7.2	2.37	1.5	3.62	51.30	1.33	3.21	ACMR _{20%} 1.56	ACMR _{20%} 1.84	Pass
3Z8S	3	10.8	1.90	1.5	4.58	15.53	1.33	4.06	ACMR _{20%} 1.56	ACMR _{20%} 1.84	Pass
Mean of performance group			2.13					3.63			Pass
6Z8S	6	21.6	2.06	1.31	4.00	13.10	1.38	4.19	ACMR _{20%} 1.56	ACMR _{20%} 1.84	Pass
9Z8S	9	32.4	1.68	0.97	2.76	18.49	1.44	4.10	ACMR _{20%} 1.56	ACMR _{20%} 1.84	Pass
12Z8S	12	43.2	1.73	0.78	2.65	10.47	1.45	5.10	ACMR _{10%} 1.96	ACMR _{10%} 2.53	Pass
15Z8S	15	54	1.92	0.66	2.13	1.55	1.16	3.76	ACMR _{10%} 1.96	ACMR _{10%} 2.53	Pass
Mean of performance group			1.85					4.29			Pass

(SCBF). The performance parameters were obtained by performing nonlinear static and dynamic analyses. The safety margin collapse of all studied archetypes was calculated by performing Incremental Dynamic Analyses (IDAs) and considering four main sources of uncertainties in the evaluation process.

All individual archetypes and performance groups did pass the acceptability process of the FEMA P695 methodology. The seismic performance evaluation of Suspended Zipper Braced Frames (SZBFs) indicated that the ACMRs of performance groups with long-period archetypes was higher than short-period one. To consider various quality ratings in the four main sources of uncertainty, two values of 0.529 and 0.726 were defined for total uncertainty. The IDA results of the archetypes with the span length of 6, 7, and 8 meters indicated that there was a slight tendency between archetype heights and \hat{S}_{CT} so that with the increase in the archetypes' height, the median collapse capacity of the archetypes decreased.

The lowest ACMRs of performance groups belonged to PG-3 which was 27% and 64% more than the acceptance criteria corresponding to the total uncertainties of 0.526 and 0.726. The archetype 2Z6S had the lowest Adjusted Collapse Margin Ratio (ACMR) among all individual archetypes with a value of 2.76 which was 50% more than the acceptance value of 1.84. The process of seismic evaluation of the designed archetype revealed that the assumed R-factor of 6 for Suspended Zipper Braced Frame (SZBF) can be modified so that it was considered more than 6 for long-period archetypes.

Disclosure statement

The authors declare that they have no known competing financial interests or personal relationships that could have appeared to influence the work reported in this paper.

ORCID

Mohammad Ali Mohammad Taghizadeh  <http://orcid.org/0000-0003-2047-517X>

Abbas Karamodin  <http://orcid.org/0000-0002-1279-5256>

References

- AISC 341-10. (2010). *Seismic provisions for structural steel buildings*. Chicago: American Institute of Steel Construction.
- Applied Technology Council. (2009). *Quantification of building seismic performance Factors*. Washington: Federal Emergency Management Agency (FEMA P695).
- ASCE/SEI 7-10. (2013). *Minimum design loads for buildings and other structures*. Reston: American Society of Civil Engineers.
- Asghari, A., & Gandomi, A. H. (2016). Ductility reduction factor and collapse mechanism evaluation of a new steel knee braced frame. *Structure and Infrastructure Engineering*, 12(2), 239–255. doi:10.1080/15732479.2015.1009123
- Baker, J. W., & Allin Cornell, C. (2006). Spectral shape, epsilon and record selection. *Earthquake Engineering & Structural Dynamics*, 35(9), 1077–1095. doi:10.1002/eqe.571
- Chanda, A., & Debbarma, R. (2021). Probabilistic seismic analysis of base isolated buildings considering near and far field earthquake ground motions. *Structure and Infrastructure Engineering*, 18(1), 97–108. doi:10.1080/15732479.2020.1836000
- Fell, B. V., Kanvinde, A., Deierlein, G., Myers, A., & Fu, X. (2006). *Steel Tips, Buckling and fracture of concentric braces under inelastic cyclic loading*. Moraga: Structural Steel Education Council.
- Gogus, A., & Wallace, J. W. (2015). Seismic safety evaluation of reinforced concrete walls through FEMA P695 methodology. *Journal of Structural Engineering*, 141(10), 04015002. doi:10.1061/(ASCE)ST.1943-541X.0001221
- Hashemi Rezvani, F., Mohammad Taghizadeh, M. A., & Ronagh, H. R. (2019). Estimating the cross-sectional area of inverted-V braces required for mitigating the progressive collapse of steel intermediate moment resisting frames. *Structure and Infrastructure Engineering*, 15(8), 1075–1086. doi:10.1080/15732479.2019.1602148
- He, Z., Ou, X., Li, J., & Ou, J. (2019). Collapse safety margin-oriented seismic retrofit strategy for corroded reinforced concrete frames using fibre reinforced plastics. *Structure and Infrastructure Engineering*, 15(8), 1025–1035. doi:10.1080/15732479.2019.1594312
- Hsiao, P.-C., Lehman, D. E., & Roeder, C. W. (2012). Improved analytical model for special concentrically braced frames. *Journal of Constructional Steel Research*, 73, 80–94. doi:10.1016/j.jcsr.2012.01.010
- Jahangiri, V., & Yazdani, M. (2021). Seismic reliability and limit state risk evaluation of plain concrete arch bridges. *Structure and Infrastructure Engineering*, 17(2), 170–190. doi:10.1080/15732479.2020.1733030
- Karamanci, E., & Lignos, D. G. (2014). Computational approach for collapse assessment of concentrically braced frames in seismic regions. *Journal of Structural Engineering*, 140(8), 1–15. doi:10.1061/(ASCE)ST.1943-541X.0001011
- Khatib, I. F., Mahin, S. A., & Pister, K. S. (1988). *Seismic behavior of concentrically braced steel frames*. Berkeley: Earthquake Engineering Research Center, University of California.
- Kildashti, K., & Mirghaderi, R. (2017). A case study on the assessment of response modification coefficient and earthquake-induced collapse potential of a high-rise setback tower. *Structure and Infrastructure Engineering*, 13(9), 1212–1229. doi:10.1080/15732479.2016.1258428
- Kim, J., Cho, C., Lee, K., & Lee, C. (2008). *Design of zipper column in inverted V braced steel frames*. Paper presented at the 14th World Conference on Earthquake Engineering, Beijing, China.
- Mazzoni, S., McKenna, F., Scott, M. H., & Fenves, G. L. (2006). *OpenSees command language manual*. *Pacific Earthquake Engineering Research (PEER) Center*, 264, 137–158.
- Muir, L., & Duncan, C. J. (2011). *The AISC 2010 Specification and the 14th Edition Steel Construction Manual [Paper presentation]*. The Structures Congress 2011. doi:10.1061/41171(401)58
- Nassani, D. E., Hussein, A. K., & Mohammed, A. H. (2017). Comparative response assessment of steel frames with different bracing systems under seismic effect. *Structures*, 11, 229–242. doi:10.1016/j.istruc.2017.06.006
- Okazaki, T., Lignos, D. G., Hikino, T., & Kajiwara, K. (2013). Dynamic response of a chevron concentrically braced frame. *Journal of Structural Engineering*, 139(4), 515–525. doi:10.1061/(ASCE)ST.1943-541X.0000679
- Ozcelik, Y., Saritas, A., & Clayton, P. M. (2016). Comparison of chevron and suspended-zipper braced steel frames. *Journal of Constructional Steel Research*, 119, 169–175. doi:10.1016/j.jcsr.2015.12.019
- Pacific Earthquake Engineering Research Center. (2010). *Guidelines for performance-based seismic design of tall buildings*. Berkeley, California: PEER. (Report No. 2017/06).
- Patil, D., & Sangle, K. (2015). *Behaviour of different bracing systems in high rise 3-D benchmark building under seismic loadings [Paper presentation]*. The 6th International Conference on Structural Engineering and Construction Management, Kandy, Sri Lanka.
- Rahimi, R., Banan, M. R., & Banan, M. R. (2016). Lateral cyclic behavior of zipper braced frames-considering connection details. *International Journal of Steel Structures*, 16(1), 11–21. doi:10.1007/s13296-016-3002-3

- Razavi, M., & Sheidaii, M. (2012). Seismic performance of cable zipper-braced frames. *Journal of Constructional Steel Research*, 74, 49–57. doi:10.1016/j.jcsr.2012.02.007
- Schachter, M., & Reinhorn, A. (2007). *Analytical modeling of zipper frames subjected to shaking table testing*. Structural Engineering Research Frontiers, 1–10. doi:10.1061/40944(249)30
- Tirca, L., & Chen, L. (2012). The influence of lateral load patterns on the seismic design of zipper braced frames. *Engineering Structures*, 40, 536–555. doi:10.1016/j.engstruct.2012.03.017
- Tirca, L., & Tremblay, R. (2004). *Influence of building height and ground motion type on the seismic behaviour of zipper concentrically braced steel frames*. Paper presented at the 13th World Conference on Earthquake Engineering.
- Uriz, P. (2005). *Towards earthquake resistant design of concentrically braced steel structures*. Berkeley: University of California.
- Uriz, P., Filippou, F. C., & Mahin, S. A. (2008). Model for cyclic inelastic buckling of steel braces. *Journal of Structural Engineering*, 134(4), 619–628. doi:10.1061/(ASCE)0733-9445(2008)134:4(619)
- Vamvatsikos, D., & Cornell, C. A. (2002). Incremental dynamic analysis. *Earthquake Engineering & Structural Dynamics*, 31(3), 491–514. doi:10.1002/eqe.141
- Yang, C.-S. (2006). *Analytical and experimental study of concentrically braced frames with zipper struts* (Doctoral dissertation). Georgia Institute of Technology. <https://repository.gatech.edu/server/api/core/bitstreams/1a23a025-7ba9-4bc5-9c78-23f87d435eb2/content>.
- Yang, C.-S., Leon, R. T., & DesRoches, R. (2008). Design and behavior of zipper-braced frames. *Engineering Structures*, 30(4), 1092–1100. doi:10.1016/j.engstruct.2007.06.010
- Zahrai, S. M., Pirdavari, M., & Farahani, H. M. (2013). Evaluation of hysteretic behavior of eccentrically braced frames with zipper-strut upgrade. *Journal of Constructional Steel Research*, 83, 10–20. doi:10.1016/j.jcsr.2012.12.017

Nomenclature

$ACMR$	Adjusted Collapse Margin Ratio
\overline{ACMR}	The average value of $ACMRs$
$ACMR_{20\%}$	Acceptable value of the $ACMR$ corresponding to an acceptable collapse probability of 20%.
$ACMR_{10\%}$	Acceptable value of the $ACMR$ corresponding to an acceptable collapse probability of 10%.
ASCE	American Society of Civil Engineers
ASTM	American Society for Testing and Materials
CBF	Chevron Braced Frame
CMR	Collapse Margin Ratio
EBF	Eccentrically Braced Frame
ELF	Equivalent Lateral Force
FEMA	Federal Emergency Management Agency
HSS	Hollow Structural Sections
IDA	Incremental Dynamic Analyses
IM	Intensity Measure
IVF	Inverted V-Braced Frame
KBF	Knee Braced Frames
MRF	Moment Resisting Frame
OBF	Ordinary Braced Frame

PG	Performance Groups
RSA	Response Spectrum Analysis
SBF	Special Braced Frame
SCBF	Special Steel Concentrically Braced Frame
SDC	Seismic Design Category
SRSS	Square Root of the Sum of Squares
SSF	Spectral Shape Factors
SZBF	Suspended Zipper-Braced Frame
VBF	V- Braced Frame
ZBF	Zipper Braced Frame

List of symbols

A_g	Gross area
b	Strain-hardening ratio
C_d	Deflection amplification factor
C_s	Seismic response coefficient
C_u	Upper-limit period coefficient
F_y	Specified minimum yield stress
F_{cre}	Critical stress
I_e	Importance factor
R	Response modification coefficient
R_y	The ratio of the expected yield stress to the specified minimum yield stress
\hat{S}_{CT}	Median 5%-damped spectral acceleration of the collapse level ground motions
S_{MT}	5%-damped spectral acceleration of the maximum Considered earthquake
S_{DS}	Design, 5% damped spectral response acceleration parameter at short periods
S_{MS}	The MCE_R , 5 percent damped, spectral response acceleration parameter at short periods adjusted for site class effects
S_1	Mapped MCE_R , 5 percent damped, spectral response acceleration parameter at a period of 1 second
S_{D1}	Design, 5% damped spectral response acceleration parameter at a period of 1 second
S_S	Mapped MCE_R , 5 percent damped, spectral response acceleration parameter at short periods
$S_T(T)$	The 5% damped spectral acceleration at the building's fundamental period
T	The fundamental period of the building
T_a	The approximate fundamental period of the building
V	Total design lateral force at the base
V_{RSA}	Modal base shear
ρ	Redundancy factor
λ_{hd}	Limiting slenderness parameter for highly ductile members
μ_T	Period-based ductility
β_{DR}	Design requirements-related collapse uncertainty
β_{MDL}	Record-to-record collapse uncertainty
β_{TD}	Modeling-related collapse uncertainty
β_{TOT}	Test data-related collapse uncertainty
δ_u	Total system collapse uncertainty
δ_y	Ultimate roof displacement
δ_y^{eff}	Effective yield roof displacement
Ω_0	Overstrength factor
Ω	Calculated overstrength of an archetype

Appendix A

Table A1. Designed member sizes for archetypes.

Archetype ID	Story	Elements			
		Braced beams	Braced columns	Braces	Zipper
2Z6S	2	W10X45	W10X19	HSS7X7X5/8	HSS6X6X1/2
	1	W10X45	W10X45	HSS6X6X3/8	
2Z7S	2	W10X68	W10X19	HSS8X8X5/8	HSS6X6X1/2
	1	W10X68	W10X45	HSS6X6X3/8	
2Z8S	2	W10X100	W10X19	W10X100	HSS7X7X5/8
	1	W10X100	W10X68	HSS6X6X5/8	
3Z6S	3	W10X45	W10X19	W10X88	W10X68
	2	W10X45	W10X68	HSS6X6X3/8	HSS7X7X5/8
3Z7S	1	W10X45	W10X68	HSS7X7X1/2	
	3	W10X68	W10X19	W10X112	W10X88
3Z8S	2	W10X68	W10X88	HSS6X6X5/8	HSS7X7X5/8
	1	W10X68	W10X88	HSS7X7X1/2	
6Z6S	3	W10X100	W10X19	W12X106	W10X100
	2	W10X100	W10X88	HSS7X7X1/2	HSS9X9X5/8
6Z7S	1	W10X100	W10X100	HSS7X7X5/8	
	6	W10X45	W10X19	W12X210	W14X233
	5	W12X120	W14X145	HSS7X7X1/2	W12X190
	4	W10X45	W14X145	HSS7X7X1/2	W12X152
	3	W10X45	W14X159	HSS7X7X5/8	W12X96
	2	W10X45	W14X176	HSS7X7X5/8	W12X50
6Z7S	1	W10X45	W14X193	HSS7X7X5/8	
	6	W10X68	W10X19	W12X252	W14X257
	5	W12X136	W14X176	HSS7X7X5/8	W12X210
	4	W10X68	W14X193	HSS7X7X5/8	W12X170
	3	W10X68	W14X193	HSS8X8X5/8	W12X120
	2	W10X68	W14X211	HSS8X8X5/8	W10X68
6Z8S	1	W10X68	W14X233	HSS8X8X5/8	
	6	W10X100	W10X19	W12X279	W14X311
	5	W12X152	W14X193	HSS8X8X5/8	W12X252
	4	W10X100	W14X211	HSS8X8X5/8	W12X190
	3	W10X100	W14X233	HSS9X9X5/8	W12X136
	2	W10X100	W14X257	HSS9X9X5/8	W10X68
9Z6S	1	W10X100	W14X283	HSS9X9X5/8	
	9	W10X45	W10X19	W12X305	W14X342
	8	W12X170	W14X211	HSS6X6X5/8	W14X311
	7	W10X45	W14X211	HSS6X6X5/8	W14X283
	6	W10X45	W14X233	HSS6X6X5/8	W14X233
	5	W10X45	W14X233	HSS7X7X1/2	W14X193
	4	W10X45	W14X257	HSS7X7X1/2	W12X152
	3	W10X45	W14X257	HSS8X8X1/2	W12X106
	2	W10X45	W14X283	HSS8X8X1/2	W10X68
9Z7S	1	W10X45	W14X283	HSS8X8X5/8	
	9	W10X68	W10X19	W12X336	W14X370
	8	W12X170	W14X233	HSS7X7X1/2	W14X342
	7	W10X68	W14X233	HSS7X7X1/2	W14X283
	6	W10X68	W14X257	HSS7X7X1/2	W14X257
	5	W10X68	W14X257	HSS7X7X5/8	W14X193
	4	W10X68	W14X283	HSS7X7X5/8	W12X152
	3	W10X68	W14X283	HSS8X8X1/2	W12X106
	2	W10X68	W14X311	HSS8X8X1/2	W10X68
9Z8S	1	W10X68	W14X311	HSS8X8X5/8	
	9	W10X100	W10X19	W14X398	W14X500
	8	W12X230	W14X311	HSS8X8X1/2	W14X455
	7	W10X100	W14X311	HSS8X8X1/2	W14X398
	6	W10X100	W14X342	HSS8X8X5/8	W14X311
	5	W10X100	W14X342	HSS8X8X5/8	W14X257
	4	W10X100	W14X370	HSS8X8X5/8	W14X193
	3	W10X100	W14X370	HSS9X9X5/8	W12X136
	2	W10X100	W14X398	HSS9X9X5/8	W10X68
12Z6S	1	W10X100	W14X426	HSS9X9X5/8	
	12	W10X45	W10X19	W14X370	W14X455
	11	W12X210	W14X283	HSS6X6X5/8	W14X426
	10	W10X45	W14X283	HSS6X6X5/8	W14X398
	9	W10X45	W14X283	HSS6X6X5/8	W14X370
	8	W10X45	W14X398	HSS6X6X5/8	W14X342
	7	W10X45	W14X398	HSS7X7X5/8	W14X283
	6	W10X45	W14X455	HSS7X7X5/8	W14X257
5	W10X45	W14X455	HSS7X7X5/8	W14X211	
4	W10X45	W14X500	HSS8X8X5/8	W12X152	

(continued)

Table A1. Continued.

Archetype ID	Story	Elements			
		Braced beams	Braced columns	Braces	Zippers
12Z7S	3	W10X45	W14X500	HSS8X8X5/8	W12X120
	2	W10X45	W14X550	HSS10X10X5/8	W10X68
	1	W10X45	W14X550	HSS10X10X5/8	-----
	12	W10X68	W10X19	W14X455	W14X550
	11	W14X283	W14X311	HSS6X6X5/8	W14X550
	10	W10X68	W14X342	HSS6X6X5/8	W14X455
	9	W10X68	W14X342	HSS7X7X5/8	W14X426
	8	W10X68	W14X426	HSS7X7X5/8	W14X370
	7	W10X68	W14X426	HSS7X7X5/8	W14X342
	6	W10X68	W14X455	HSS7X7X5/8	W14X283
12Z8S	5	W10X68	W14X455	HSS7X7X5/8	W14X233
	4	W10X68	W14X500	HSS8X8X5/8	W14X193
	3	W10X68	W14X500	HSS8X8X5/8	W12X136
	2	W10X68	W14X550	HSS10X10X5/8	W10X68
	1	W10X68	W14X550	HSS10X10X5/8	-----
	12	W10X100	W10X19	W14X550	W14X605
	11	W14X342	W14X455	HSS9X9X5/8	W14X550
	10	W10X100	W14X455	HSS9X9X5/8	W14X500
	9	W10X100	W14X455	HSS9X9X5/8	W14X455
	8	W10X100	W14X500	HSS9X9X5/8	W14X398
15Z6S	7	W10X100	W14X500	HSS9X9X5/8	W14X342
	6	W10X100	W14X500	HSS9X9X5/8	W14X283
	5	W10X100	W14X500	HSS9X9X5/8	W14X233
	4	W10X100	W14X550	HSS9X9X5/8	W14X193
	3	W10X100	W14X550	HSS9X9X5/8	W12X136
	2	W10X100	W14X605	HSS10X10X5/8	W10X68
	1	W10X100	W14X605	HSS10X10X5/8	-----
	15	W10X45	W10X19	W14X370	W14X455
	14	W12X210	W14X257	HSS5X5X3/8	W14X426
	15Z7S	13	W10X45	W14X283	HSS5X5X3/8
12		W10X45	W14X283	HSS6X6X3/8	W14X370
11		W10X45	W14X283	HSS6X6X3/8	W14X342
10		W10X45	W14X283	HSS6X6X3/8	W14X342
9		W10X45	W14X311	HSS6X6X3/8	W14X311
8		W10X45	W14X311	HSS6X6X1/2	W14X283
7		W10X45	W14X311	HSS6X6X1/2	W14X233
6		W10X45	W14X342	HSS6X6X1/2	W14X193
5		W10X45	W14X342	HSS6X6X1/2	W12X170
4		W10X45	W14X342	HSS6X6X1/2	W12X136
15Z8S	3	W10X45	W14X370	HSS6X6X5/8	W12X96
	2	W10X45	W14X370	HSS6X6X5/8	W10X68
	1	W10X45	W14X370	HSS6X6X5/8	-----
	15	W10X68	W10X19	W14X398	W14X500
	14	W14X257	W14X283	HSS6X6X3/8	W14X455
	13	W10X68	W14X283	HSS6X6X3/8	W14X426
	12	W10X68	W14X311	HSS6X6X3/8	W14X398
	11	W10X68	W14X311	HSS6X6X3/8	W14X370
	10	W10X68	W14X311	HSS6X6X1/2	W14X342
	9	W10X68	W14X342	HSS6X6X1/2	W14X311
15Z8S	8	W10X68	W14X342	HSS6X6X1/2	W14X283
	7	W10X68	W14X342	HSS6X6X1/2	W14X233
	6	W10X68	W14X370	HSS6X6X1/2	W14X211
	5	W10X68	W14X370	HSS6X6X5/8	W12X170
	4	W10X68	W14X370	HSS6X6X5/8	W12X136
	3	W10X68	W14X398	HSS6X6X5/8	W12X96
	2	W10X68	W14X398	HSS6X6X5/8	W10X68
	1	W10X68	W14X398	HSS6X6X5/8	-----
	15	W10X100	W10X19	W14X550	W14X550
	14	W14X342	W14X342	HSS6X6X5/8	W14X550
13	W10X100	W14X342	HSS6X6X5/8	W14X500	
12	W10X100	W14X342	HSS6X6X5/8	W14X455	
11	W10X100	W14X370	HSS6X6X5/8	W14X426	
10	W10X100	W14X370	HSS7X7X1/2	W14X370	
9	W10X100	W14X398	HSS7X7X1/2	W14X342	
8	W10X100	W14X398	HSS7X7X1/2	W14X311	
7	W10X100	W14X398	HSS7X7X1/2	W14X257	
6	W10X100	W14X426	HSS7X7X1/2	W14X233	
5	W10X100	W14X426	HSS7X7X5/8	W12X190	
4	W10X100	W14X455	HSS7X7X5/8	W12X136	
3	W10X100	W14X455	HSS7X7X5/8	W12X96	
2	W10X100	W14X500	HSS7X7X5/8	W10X68	
1	W10X100	W14X500	HSS7X7X5/8	-----	